Check for updates

ENVIROMENTAL STUDIES

Nonliving respiration: Another breath in the soil?

Clémentin Bouquet[1]†, Benoit Kéraval[1]†, Mounir Traikia[2,3], Gaël Alvarez[4], Fanny Perrière[1], Anne-Hélène Le Jeune[1], Hermine Billard[1], Jonathan Colombet[1], Sandrine Revaillot[4], Sébastien Fontaine[4]‡, Anne-Catherine Lehours[1]*‡

Copyright © 2025 The Authors, some rights reserved; exclusive licensee American Association for the Advancement of Science. No claim to original U.S. Government Works. Distributed under a Creative Commons Attribution NonCommercial License 4.0 (CC BY-NC).

The present study challenges the traditional view that the respiration of organic carbon to CO_2 is an exclusively intracellular process, revealing that organic compound respiration can occur spontaneously in an extracellular context in soils. Using ^1H nuclear magnetic resonance spectroscopy to analyze the dynamics of the sterile soil exometabolomes alongside C-CO_2 flux analyses and sterile soil fuel cells, we show that soil catalysts facilitate a diverse array of substrate-driven reactions, leading to the complete oxidation of organic compounds to CO_2 with O_2 consumption. Our results indicate that soil particles are capable of transferring electrons from substrates to the final acceptor, thereby sustaining metabolism-like processes independently of living cells. Notably, some soil catalysts and induced respiration remain stable for more than 6 years. These findings support the coexistence of cellular and noncellular metabolic pathways in soil respiration.

INTRODUCTION

In a universe that is constantly tending toward greater disorder, living organisms must actively create and maintain order to survive, a trait that fundamentally distinguishes them from nonliving matter. To combat this inherent drive toward entropy, cells must carry out a never-ending stream of chemical reactions. In heterotrophic cells, the essence of these cascades of redox reactions, known as respiration, is the oxidation of small organic molecules (e.g., organic acids, amino acids, and sugars) that fuel cells with the energy stored in their chemical bonds and provide many other molecules that the cell needs. The captured electrons are transferred to a terminal electron acceptor, namely molecular oxygen (O_2) in aerobic respiration, and CO_2 and H_2O are the end products of these reactions. These cellular biochemical reactions are organized in such a way as to make them possible at low temperatures and to recover the energy released.

In addition to the functions of respiration in cell bioenergetics, this cellular mechanism is crucial for forecasting the global carbon cycle (C) and its climate feedbacks. In terrestrial ecosystems, in particular, soil respiration is the primary process by which CO_2 fixed by photosynthetic organisms in organic matter (OM) is recycled into the atmosphere (*1*, *2*). With soil OM containing three times as much carbon as the atmosphere, a small change in soil respiration can have a major impact on atmospheric CO_2 and Earth's temperature (*3*–*5*). This has prompted scientists since the early 20th century to study the catabolic activities of soil microbes and their response to environmental factors (*6*). Unexpectedly, several studies have found that soil respiration is not always connected to the size and composition of the microbial biomass, as experimental reductions in these microbial components have moderate effects on the respiration rate [e.g., (*7*, *8*)]. It has also been observed that substantial CO_2 emissions can persist for several weeks in soils where microbial life has been substantially reduced or even become undetectable by exposure to toxics ($ClCH_3$ and orange acridine), γ-irradiation, or autoclaving (*7*, *9*–*13*). Such CO_2 emissions cannot be explained by the activity of surviving microbes that would be present in small quantities in soils, unless we consider unrealistic cellular respiratory activity (*13*). Furthermore, the isotopic signature of CO_2 emissions ($\delta^{13}C = -75.4 \pm 2.8‰$) from sterilized soils with an excess of substrates indicates isotope fractionation during the conversion process of organic C ($\delta^{13}C = -27.4 \pm 0.4‰$) to CO_2 (*12*), incompatible with cell-derived respiration (*14*, *15*).

Various noncellular processes have been proposed as potential contributors to CO_2 emissions in sterile soils such as (i) single catalytic reactions induced by reactive oxygen species and/or metals such as iron (*16*) or supported by decarboxylases released during cell lysis (*17*), (ii) complete mineralization of organic compounds supported by extracellular oxidative metabolisms (EXOMETs) (*12*, *13*). EXOMETs are distinguished from the other processes by their complexity and persistence over time. EXOMETs, according to the definition proposed by Maire *et al.* (*13*), involve numerous coupled redox reactions carried out by soil-stabilized enzymes and/or abiotic catalysts (clay and metals), reconstituting an equivalent of a cell respiration process capable of converting organic compounds such as glucose into CO_2 with electron transfer to O_2. The EXOMET hypothesis is challenging. The respiratory machinery is rather complicated and involves numerous respiratory-mediating endoenzymes whose functioning depends on a variety of redox cofactors that need to be regenerated {e.g., NAD^+ [nicotinamide adenine dinucleotide (oxidized form)]}, their location close to other enzymes, and the physiological properties of the cell (e.g., redox potential) (*18*). Owing to this complexity and the fact that cellular enzymes are superbly crafted but vulnerable catalysts, respiration is currently considered to be a strictly intracellular metabolic process.

In the present study, we have combined exometabolomics and isotope approaches in medium-term (~6 months) and long-term (>6 years) experiments in soil microcosms, as well as the construction of fuel cells using sterile soils, to demonstrate that soils contain catalysts that are stable over years and capable of generating a chain of redox reactions that lead to the complete mineralization of various organic compounds to CO_2 and electron transfer to oxygen. These results show that the respiration of organic compounds is not

[1]CNRS, LMGE, Université Clermont Auvergne, F-63000 Clermont-Ferrand, France. [2]CNRS, ICCF, Université Clermont Auvergne, F-63000 Clermont-Ferrand, France. [3]PFEM, MetaboHUB Clermont, Université Clermont Auvergne, Clermont-Ferrand, France. [4]INRAE, VetAgro Sup, UMR Ecosystème Prairial, Université Clermont Auvergne, 63000 Clermont-Ferrand, France.
*Corresponding author. Email: a-catherine.lehours@uca.fr
†These authors contributed equally to this work.
‡These authors contributed equally to this work.

Downloaded from https://www.science.org on November 28, 2026

a cell-specific process and that it can spontaneously occur in an extracellular context in soils.

RESULTS AND DISCUSSION

Noncellular processes generate both the production and consumption of various metabolites

To study whether the sole action of soil catalyzers is able to sustain chains of chemical reactions, we examined the exometabolomes of sterilized and nonsterilized soils incubated for 163 days in the dark at 20°C. The soils were sterilized by γ-irradiation at 45 kilograys (kGy), which is an effective sterilizing agent in the soil particularly at doses above 20 kGy (*19*, *20*) and does not disrupt the soil structure and chemistry as much as autoclaving (*20*, *21*). Three substrate treatments were applied to sterilized soils to test the ability of soil catalyzers to degrade different substrates of varying complexity: no substrate addition [hereafter referred to as irradiated soil (IS)] or the addition of ^{13}C-citrate (C-IS) or ^{13}C-glucose (G-IS). All manipulations were carried out under strict sterile conditions, and the sterility of IS, C-IS, and G-IS samples was checked using live/dead cell staining coupled to flow cytometry analysis (fig. S1), an approach previously validated in this research (*12*, *22*). The extracellular fraction of molecules that are inferred to be produced and/or used in soil, i.e., the exometabolome, was profiled at six dates during incubation using untargeted metabolomics, a robust approach to provide comprehensive analyses of complex extracts (*23*, *24*). We use proton nuclear magnetic resonance spectroscopy (^{1}H NMR) to track the dynamics of the water-extractable fraction of exometabolites with a molecular weight <3 kDa at the exometabolome scale. Water is an excellent solvent for examining total extractable OM in soils (*23*), and the 0- to 3-kDa size class of metabolites, including small- to mid-sized molecules (e.g., amino acids, carbohydrates, and organic acids), represents most of the compounds of dissolved OM in soils (*25*). Chemical information encoded in NMR data was explored after manual grouping (*26*, *27*) of the spectral responses into variable size buckets (i.e., a spectral region corresponding to a peak observed in NMR) subjected to statistical data analysis after a normalization step.

A total of 177 and 506 distinct buckets between 0 and 10 parts per million (ppm) of NMR spectra were identified in the exometabolome of nonsterilized [i.e., hereafter referred to as living soil (LS)] and IS samples, respectively (fig. S2). At the start of incubation (T1 = 0.2 days after soil rewetting), the molecular richness and diversity were higher in IS samples than in LS samples (Fig. 1, A and B). This is presumably due to the release of cellular metabolites from dead biomass and/or the degradation of OM in the soil following γ-irradiation.

Downloaded from https://www.science.org on November 28, 2026

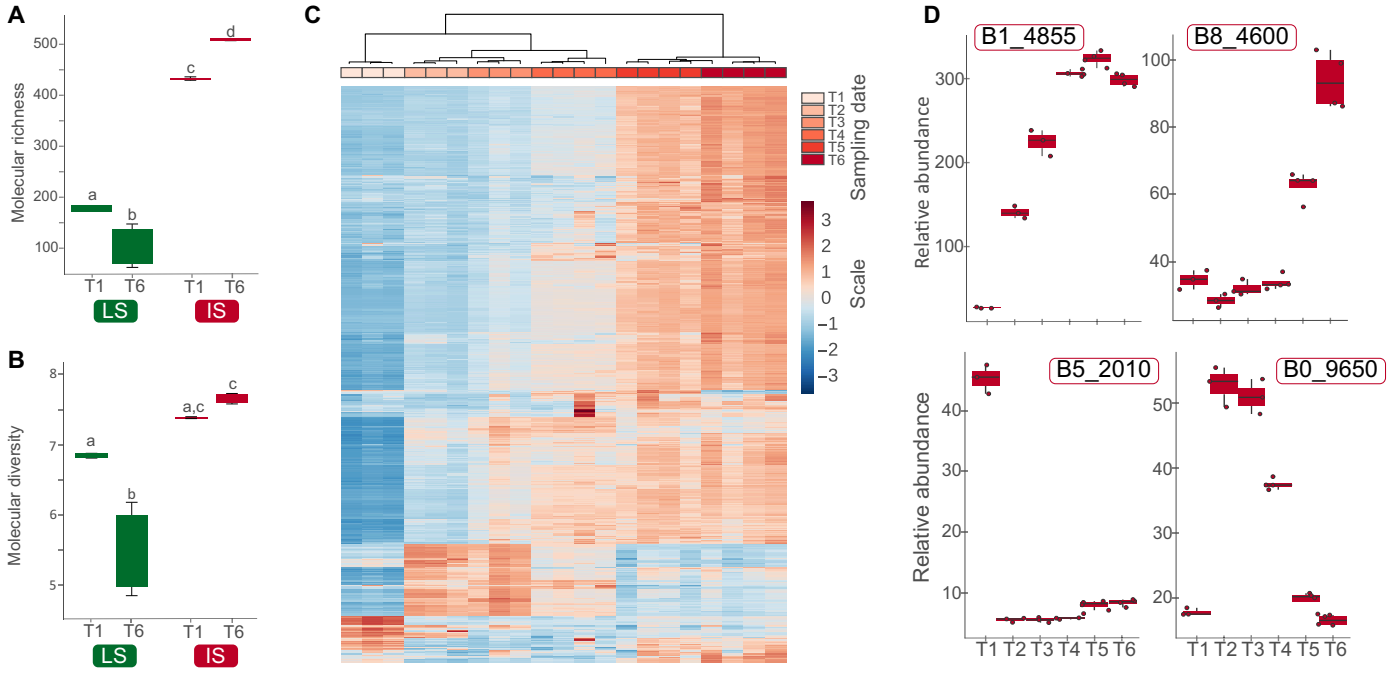


Fig. 1. Richness and diversity of the global exometabolome in nonsterilized and sterilized soils and dynamics of selected buckets in IS microcosms. (**A**) Molecular richness (number of non-null buckets) and (**B**) molecular diversity (expressed by the Shannon diversity index) in the water-extractable fraction of exometabolites with molecular weight <3 kDa in nonsterilized soil (LS) and sterilized (IS) soil at the beginning (T1 = 0.2 days) and end (T6 = 163 days) of the incubation period. The mixed effects model was applied to test for differences between the two groups using the Holm-Sidak post hoc test. (**C**) Heatmap showing the relative intensities of the water-extractable fraction of exometabolites with molecular weights <3 kDa in sterilized soil (IS) at the different sampling dates. Relative abundance is normalized to the concentration of the reference molecule during ^{1}H NMR processing. The shades of red and blue indicate increasing and decreasing intensities, respectively. The color scale represents the magnitude of the change. Individual samples are plotted on the horizontal axis, and buckets are plotted on the vertical axis. Hierarchical clustering of the samples was performed using the Euclidean distance metric and Ward's clustering method. (**D**) Temporal dynamics of the relative abundance of four selected buckets (B1_4855, B8_4600, B5_2010, and B0_9650) in sterilized soil (IS). Relative abundance is normalized to the concentration of the reference molecule during ^{1}H NMR processing. The name of each bucket corresponds to its mean chemical shift (for example, B0_9560 refers to the bucket identified with a mean chemical shift of 0.9560 ppm). Data are presented as the means, minimum, and maximum for the four replicate samples by sampling date. T1 = 0.2 days, T2 = 3 days, T3 = 6 days, T4 = 17 days, T5 = 100 days, and T6 = 163 days.

In LS samples, both indicators decreased during incubation (Fig. 1, A and B), consistent with evidence that microbial decomposition reduces the molecular diversity of soil OM (*28*). In contrast, exometabolite diversification was promoted over time in sterilized soil samples (Fig. 1, A and B), demonstrating that the processes governing metabolite dynamics in the LS and IS microcosms are quite different. Although a general trend toward exometabolite accumulation was observed in the IS, C-IS, and G-IS microcosms between T1 and T6 (Fig. 1C and fig. S3), bucket dynamics also showed a decrease in some exometabolites over time in three sterilized treatments (Fig. 1C and fig. S3). Some buckets show changing dynamics over time, increasing and then decreasing or vice versa, suggesting that molecules undergo consumption and production dynamics (Fig. 1D). Sorption or desorption of molecules from the solid phase of the soil could contribute to short-term dynamics but not over a period of 160 days. Studies of sorption/desorption kinetics for a wide range of chemical compounds show that these processes stabilize within a few hours to days, after which equilibrium between the solid and liquid phases is reached (*29*–*31*). We conclude that the catalysts present in sterilized soils are capable of sustaining a wide range of chemical reactions that produce and consume molecules over several months. Some of these reactions can involve the exchange of molecules, creating metabolism-like reaction chains in an extracellular context.

Chemical reactions in sterilized soils have ordered temporal dynamics controlled by substrates

The temporal dynamics of exometabolome fingerprints in sterilized (IS, C-IS, and G-IS) and nonsterilized (LS) soils were represented using unsupervised two-dimensional principal components analysis (PCA), with each point in the PCA score plots representing an individual replicate sample (Fig. 2). Irrespective of sampling date, LS samples showed different exometabolome profiles compared to sterilized soils (Fig. 2A). For IS, C-IS, and G-IS, a high degree of exometabolome consistency was observed between independent replicates at each sampling date (Fig. 2B and fig. S4). In contrast, in LS, biological variation resulted in greater heterogeneity between biological replicates, particularly in the later stages of incubation (fig. S5).

In sterilized soils, the NMR data show time-ordered trajectories of metabolic fingerprint dynamics that diverge progressively between T1 and T6, with the exometabolome composition at one sampling date being closer to that of the previous and subsequent dates than to the others (Fig. 2B and fig. S4). The addition of ^{13}C-glucose and ^{13}C-citrate (3 gC kg^{-1} soil), representing less than 10% of the soil C content (39 gC kg^{-1} soil), resulted in a notable divergence of exometabolite fingerprints compared to unamended sterilized soil (Fig. 2C). Furthermore, exometabolomes and their trajectories diverged between G-IS and C-IS. These substrate-specific responses of exometabolomes indicate that the chemical reaction chains present in sterilized soils are, at least for some of them, capable of processing and transforming different carbonaceous substrates. This result is corroborated by a recent study in which the water-extractable fraction of exometabolites from IS-soil samples was analyzed using chromatography coupled with mass spectrometry (*32*). The results show that a sterile soil matrix, when incubated with glucose or citrate, can spontaneously generate intermediates of Krebs cycle, an important cell's metabolic hub (*32*).

Metabolism-like reactions in sterilized soils lead to complete oxidation of the carbonaceous organic substrates

Soil catabolic activities were also quantified for nonsterilized (LS) and sterilized soils without (IS) and with ^{13}C-citrate (C-IS) and ^{13}C-glucose (G-IS) by measuring the CO_2 and O_2 concentrations, as well as the isotopic signature of C-CO_2 (δ^{13}C-CO_2) in incubated flasks throughout the 163 days of incubation. Expectedly, LS induced CO_2 production and O_2 consumption (fig. S6). Sterilized soils also induced both gas exchanges (Fig. 3). At the beginning of the incubation period

Downloaded from https://www.science.org on November 28, 2026

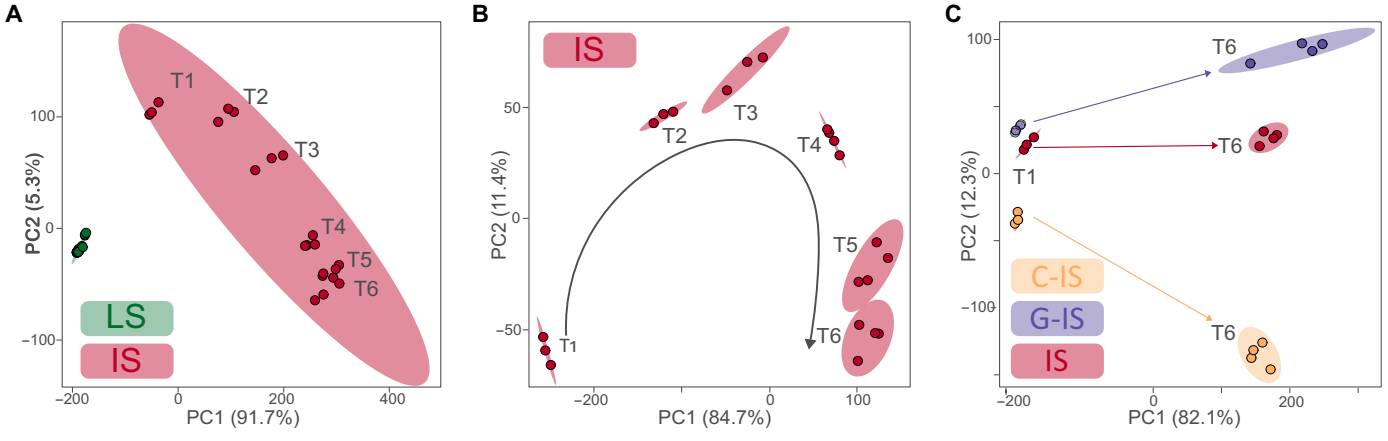


Fig. 2. Dynamics of the water-extractable fraction of exometabolites with molecular weight <3 kDa in soil microcosms, analyzed by ^{1}H NMR. (**A**) PCA of the temporal dynamics of the exometabolome in nonsterilized (LS) and sterilized (IS) soils between T1 and T6. For LS, all dates and replicates are represented, but they overlap. (**B**) PCA of the temporal dynamics of the exometabolome in IS samples between T1 and T6. (**C**) PCA of the exometabolome dynamics at T1 (0.2 days) and T6 (163 days) for IS and for sterilized soils amended with ^{13}C-glucose (G-IS) or ^{13}C-citrate (C-IS). To make the graph easier to read, only the dates T1 and T6 are shown; however, the PCA plots for C-IS and G-IS are provided in the Supplementary Materials (fig. S4). Each point on the PCA plot represents a replicate (four replicates per date and per condition) incubated in the dark at 20°C. At each sampling date, each replicate was sacrificed. Colored ellipses indicate 95% confidence regions. The two-dimensional PCA score plot shows that the first two principal components account for >94% of the variance explained with the first principal component (PC1) retaining >82.1% of the variance. The arrows in (B) and (C) have been manually added to highlight the temporal dynamics. T1 = 0.2 days, T2 = 3 days, T3 = 6 days, T4 = 17 days, T5 = 100 days, and T6 = 163 days.

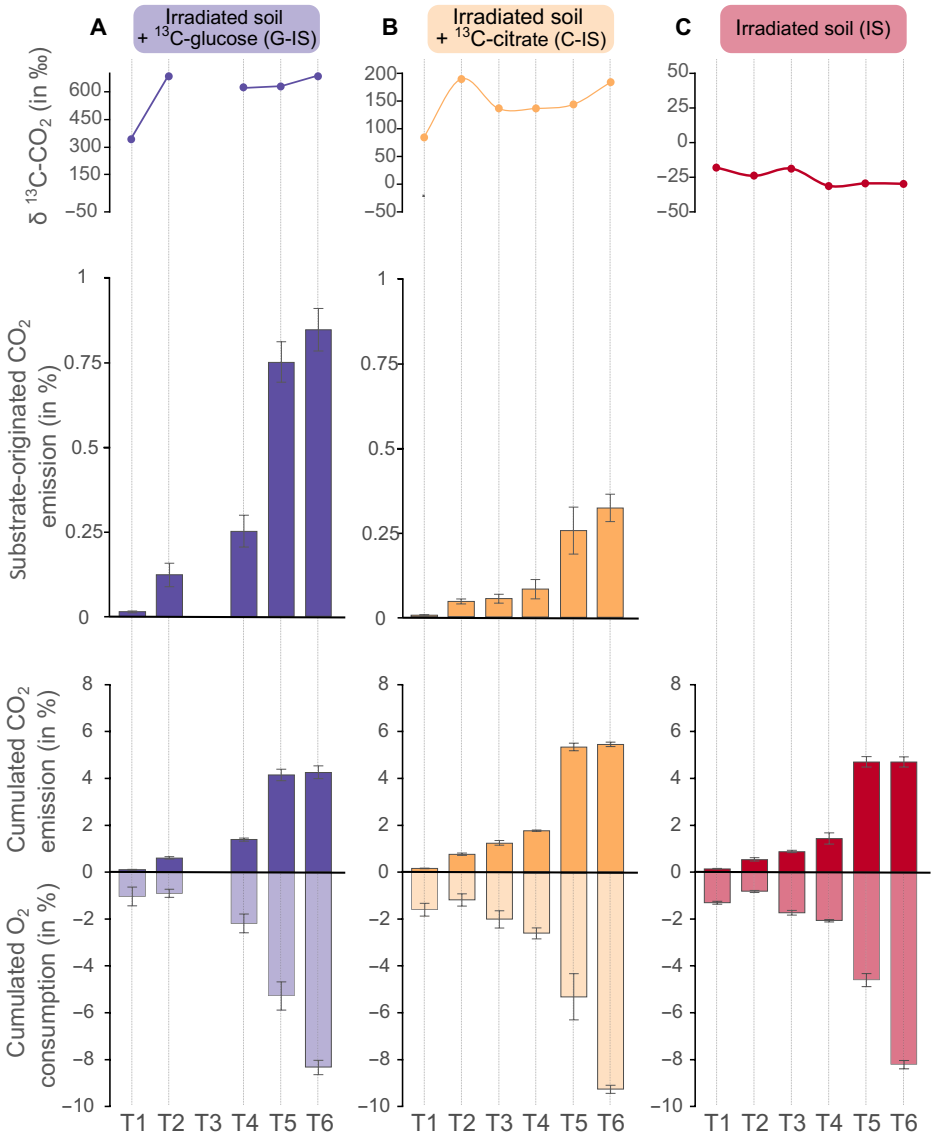


Fig. 3. Isotopic signatures of labeled and unlabeled CO_2, CO_2 emission, and O_2 consumption from sterilized soil microcosms that were amended with either ^{13}C-glucose (G-IS), ^{13}C-citrate (C-IS), or left unamended (IS). (**A**) IS amended with ^{13}C-glucose (G-IS), (**B**) IS amended with ^{13}C-citrate (C-IS), and (**C**) irradiated unamended soil (IS). The isotopic signature (δ^{13}C-CO_2) of CO_2 is shown at the top of the graph in (A) to (C) and is expressed in ‰. CO_2 emissions originating from glucose or citrate are presented in the middle graphs in (A) and (B). Total CO_2 emissions and O_2 consumption are shown in the lower graphs in (A) to (C). Results are expressed as a percentage of the microcosm atmosphere. For each sampling date (T1, T2, T3, T4, T5, and T6) and for each parameter, the mean values and standard deviations from four replicate samples are shown. Information on the T3 date for G-IS was not available. T1 = 0.2 days, T2 = 3 days, T3 = 6 days, T4 = 17 days, T5 = 100 days, and T6 = 163 days.

(T1), CO_2 emissions from IS were found to be 63.0 ± 5.8% of those in LS. This ratio then decreased rapidly and stabilized at 16.6 ± 0.5% by T6, with no significant difference observed between T2 and T6 (Fig. 3 and fig. S6). This ratio is consistent with the estimated potential contribution of EXOMETs to soil CO_2 emissions, which was found to be 12 to 50% depending on soil properties (*13*, *22*).

The addition of ^{13}C-labeled glucose or citrate induced a large increase in δ^{13}C-CO_2 values (Fig. 3, A and B) compared to unamended soils (Fig. 3C). The δ^{13}C-CO_2 values increased from 330 ± 0.8 to 685.3 ± 0.8‰ and from 84.0 ± 0.8 to 182.7 ± 0.9‰ between T1 and T6 under glucose and citrate treatments, respectively (Fig. 3, A and B). The isotopic mass balance calculation was then used to determine the CO_2 emissions directly associated with the labeled substrates. This revealed continuous CO_2 production originating from the labeled substrate during the 163-day incubation period, resulting in CO_2 accumulation from 0.012 ± 0.003 to 0.847 ± 0.063% and 0.005 ± 0.002 to 0.324 ± 0.041% under glucose and citrate treatments, respectively (Fig. 3, A and B). These results indicate that the diverse chemical reactions previously revealed in the sterilized soils (Figs. 1 and 2) can lead to the complete oxidation of molecules such as citrate, glucose, and various soil compounds.

We note that CO_2 emission is accompanied by O_2 consumption under all incubation conditions in sterilized soil (Fig. 3). The respiratory quotient, which varied from 0.51 to 1.02 as a function of time

Downloaded from https://www.science.org on November 28, 2026

and experimental conditions, is in the range of that obtained by Maire *et al.* (*13*). Direct oxidation of organic substrates by O_2, which has a triplet ground state, is rare because of the generally high energy barrier for electron transfer from the organic substrate to the oxidant (*33*). To overcome the unfavorable kinetics associated with direct aerobic oxidation, cells use a complex machinery involving cascades of reactions, electron transfer molecules such as NADH (reduced form of NAD^+) and $FADH_2$ (reduced form of flavin adenine dinucleotide), and protein chains that minimize the energy barrier. Our metabolomics study (Figs. 1 and 2) suggests that the oxidation of organic substrates and electron transfers to oxygen can also occur via a cascade of redox reactions in sterilized soils. However, this cascade of redox reactions requires the capacity of soil particles and solution to transfer electrons from one reaction to the other toward oxygen, a capacity that remains to be demonstrated.

Electron transfer capacity of sterilized soils

To establish the electron transfer capacity of sterilized soils, we constructed an experimental fuel cell (Fig. 4A) inspired by soil microbial fuel cells (*34*). The principle of our single-chamber fuel cell is based on a column of sterilized soil where the upper part is exposed to oxygen from the air, while the lower part is confined to the outside, creating a decreasing oxygen gradient from the top of the cell (the cathode) to the bottom (the anode). The sterilized soil was stored at 20°C for 4.8 years before use, a period long enough for the cellular debris to become invisible under an electron microscope (*12*) and for enzymes to be inactivated (*13*).

When the fuel cell is connected, the oxygen gradient favors the capture of the electrons produced by the oxidation of organic molecules in the buried sterilized soil. The electrons collected at the anode are transported through an external circuit containing a variable resistor to the cathode, where O_2 acts as an electron acceptor (Fig. 4A). One substrate treatment (50 mM sodium pyruvate) and two control treatments [50 mM sodium chloride (NaCl) or water] were used to verify that the current produced was due to the oxidation of organic molecules. The electricity generated by the fuel cells was characterized by measuring the cell voltage (*U*) and current (*I*) across the external circuit by varying the resistance from 330 to 11,900 ohms after 9 days of fuel cell incubation. The ability of the fuel cells to generate electricity was also regularly checked over a period ranging of 20 min to 80 days after construction using a 476-ohm resistance (Fig. 4B). Closing the fuel cell circuit induced a current in all fuel cells within minutes or hours (Fig. 4, B and C), indicating that soil particles respond rapidly to the oxygen gradient: The soil particles donate electrons to the anode, and the soil particles receiving electrons at the cathode ultimately transfer them to the oxygen

Downloaded from https://www.science.org on November 28, 2026

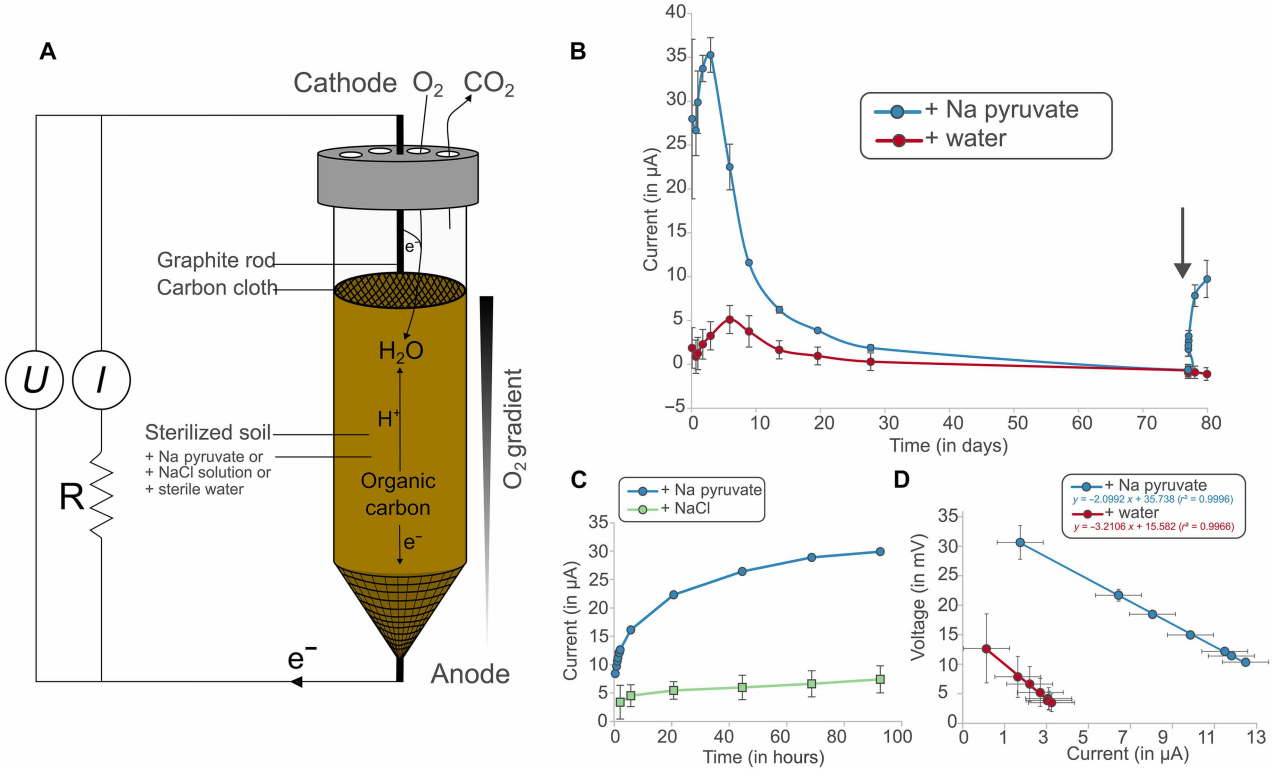


Fig. 4. Direct relationship between the electron transfer capacities of sterilized soils and substrate availability revealed by electrical activity measurements of sterilized soil fuel cells. (**A**) Schematic representation of the sterilized soil fuel cell developed in this study. The current induced by the fuel cell was measured after sterile solutions of sodium pyruvate (Na pyruvate), water, or NaCl were added at the start of the experiment. The voltage (*U*) and current (*I*) generated between the anode and the cathode were measured on the external circuit. R and e^- represent the circuit resistor and the electrons, respectively. (**B**) Current generated (in µA) as a function of time in sterilized soil fuel cells to which sodium pyruvate or water solutions were added at the start of the experiment and after 77 days (indicated by the gray arrow). (**C**) Progressive increase in current during the first 96 hours following addition of pyruvate in a sterilized soil fuel cell. NaCl solution was used as a control. (**D**) Cell voltage (in mV) versus current (in µA) curves for sterilized soil fuel cells to which sodium pyruvate or water solutions were added. The electromotive force and current of the fuel cell were determined by connecting the fuel cell to decreasing resistances (from 330 to 11,900 ohms) after 216 hours.

(Fig. 4A). The fuel cells also show a classic negative linear relationship between the voltage and the current, which is explained by the internal resistance, given by the slope of the regression line (Fig. 4D and fig. S7). Compared to the water or NaCl treatments, the addition of sodium pyruvate induced a rapid (within 20 min) and strong increase in both the current and voltage (Fig. 4, B and C). No significant difference in *I* values was found between the two control treatments (water and NaCl; table S1), confirming that sodium pyruvate–induced electricity was promoted by the addition of pyruvate and not by the addition of Na^+ (Fig. 4, B and C). The current reached a peak (35.3 ± 1.9 μA) 3 days after the addition of pyruvate and then decreased continuously to reach the control level (Fig. 4B). This decrease is related to the depletion of the carbonaceous substrate; adding more pyruvate increased current production (Fig. 4B). These results show that soil particles mediate electron transfer from the carbonaceous substrate to the final acceptor, in this case, oxygen.

Long-term dynamics of catabolic activity in sterilized soil are controlled by different catalyst pools

We studied the persistence of noncellular catabolic activities by incubating sterilized soil microcosms for 6.7 years. To test whether these activities could be substrate limited in the long term, two treatments were set up: one without the addition of ^{13}C-glucose (S) and one with the addition of ^{13}C-glucose (S + G). The CO_2 emission rate and δ^{13}C-CO_2 were measured at nine sampling times across three replicates per condition. The sterility of soil microcosms was verified by live/dead staining coupled with flow cytometry analysis, a cultivation approach, and observations of thin sections of soil by transmission electron microscopy (TEM). At the end of the incubation, no viable cells were detected in S and S + G (fig. S1).

The kinetics of CO_2 emission rate in microcosms S and S + G showed a sharp decrease over the first 4 days (Fig. 5A), from a maximum close to 13 μmol C-CO_2 day^{-1} after 12 hours of incubation to about 2.4 μmol C-CO_2 day^{-1} on day 4. The rate of CO_2 emission then decreased exponentially until it reached 0.27 and 0.34 μmol C-CO_2 day^{-1} in the S and S + G microcosms, respectively, on day 1125. Between the fourth and sixth year, the emission rate tended to stabilize, decreasing by only 4.9 and 1.5% per year in microcosms S and S + G, respectively.

The addition of ^{13}C-glucose increased the CO_2 emission rate only after 4 years of incubation (S + G compared to S; Fig. 5A). This suggests that the exponential decrease in CO_2 emissions during the first steps of incubation is caused by factors other than an exhaustion of carbonaceous substrates. Moreover, the increased rate of CO_2 emissions in S + G was associated with the oxidation of ^{13}C-glucose in $^{13}CO_2$ (Fig. 5B). These results show the ability of soil particles to oxidize glucose and/or its catabolites in an extracellular context for years.

We used statistical modeling to analyze CO_2 emission rate kinetics and investigate various catalyst types and lifespans supporting noncellular catalytic activities. Six different models were constrained using the CO_2 emission rate of the glucose-amended soil (Fig. 6). This treatment was used to minimize the impact of substrate limitation on the decrease in CO_2 emission rates over time. By the end of the experiment, only 2.6% of the supplied glucose had been mineralized into CO_2. To focus on the long-term behavior of the catalytic activities, the decrease in the CO_2 emission rate over the first 4 days was excluded from the analysis.

Comparisons of the competing models using Akaike's information criterion resulted in the selection of two models (models 5 and 6 in Fig. 6), which consider two different catalytic processes with contrasting persistence. For the catalytic process with the shortest persistence, the two models converge on a half-life of 71 days. This half-life is within the range observed for enzymes stabilized on soil particles, such as clays (*13*, *35*, *36*). For the second process, our results do not allow us to distinguish one model as being more relevant than the other. Model 5 assumes that the catalytic process has a limited lifetime, with a half-life of 7 years. Model 6 assumes that the catalytic process is completely stable over time. However, given that even stabilized enzymes have a half-life of well under 7 years (*13*, *35*, *36*), both models suggest that the most persistent noncellular catalytic process cannot be mediated by enzymes.

We propose that persistent catalytic processes in sterilized soils involve the activity of highly stable catalysts such as soil organominerals

Downloaded from https://www.science.org on November 28, 2026

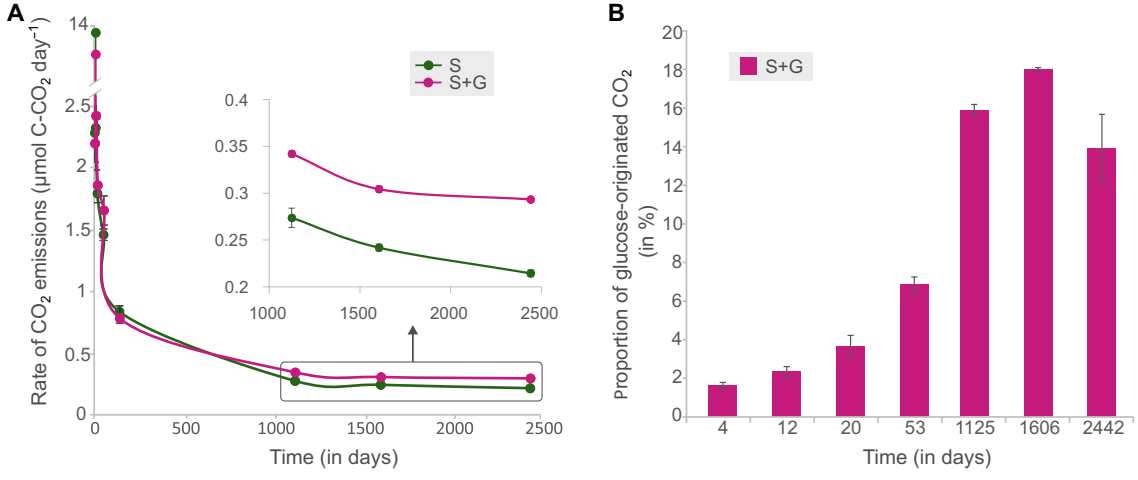


Fig. 5. Emissions of CO_2 in sterilized soils amended with ^{13}C-glucose or unamended over an incubation period of more than 6 years. (**A**) Rate of total CO_2 emissions from sterilized soils (IS) with (S + G) and without (S) the addition of ^{13}C-labeled glucose in a long-term experiment (>6 years). (**B**) Percentage of glucose-derived carbon in CO_2 emissions from sterilized soils with ^{13}C-labeled glucose (S + G). The inset in the top right corner of (A) shows an enlargement of the curves between 1125 and 2442 days. Standard deviations are shown in all plots.

A

Model	Equation	Parameter estimates				R^2	AIC
		a	k_1	b	k_2		
Model 1	$a{\cdot}e^{-k_1{\cdot}t}$	1.07 ***	0.75×10^{-2} ***	–	–	0.92	−33.51
Model 2	$a{\cdot}e^{-k_1{\cdot}t} + b{\cdot}e^{-k_2{\cdot}t}$	0.94 ***	0.97×10^{-2} ***	1.46	0.22×10^{-4}	–	–
Model 3	$a{\cdot}e^{-k_1{\cdot}t} + b{\cdot}e^{-\frac{\ln(2)}{43}{\cdot}t}$	0.22	1.61×10^{-2}	1.00	–	–	–
Model 4	$a{\cdot}e^{-k_1{\cdot}t} + b{\cdot}e^{-\frac{\ln(2)}{495}{\cdot}t}$	0.67 ***	1.56×10^{-2} *	0.43 **	–	0.94	−40.04
Model 5	$a{\cdot}e^{-k_1{\cdot}t} + b{\cdot}e^{-\frac{\ln(2)}{12{,}649}{\cdot}t}$	0.93 ***	0.98×10^{-2} ***	0.15 ***	–	0.97	−57.66
Model 6	$a{\cdot}e^{-k_1{\cdot}t} + c$	0.94 ***	0.96×10^{-2} ***	0.14 ***	–	0.97	−57.67

B

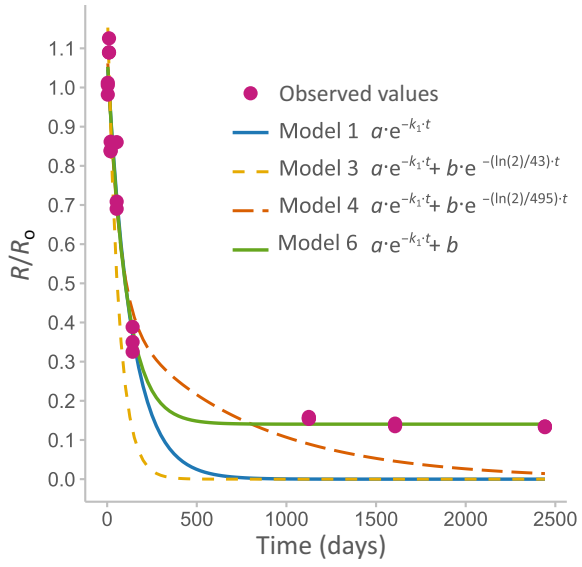


Fig. 6. Modeling the long-term dynamics of the daily CO_2 emission rate observed in IS supplemented with glucose (S + G). (**A**) The model equations and statistical results obtained after fitting the models to the data are shown. The models were fitted using the nls function in the lme4 R package. For models 2 to 5, the "port" algorithm was used as an nls parameter to constrain the k_1 estimate to a value greater than the second modeled activity kinetics decay rate. The absence of an asterisk after the estimate indicates a nonsignificant result. (**B**) Long-term dynamics of the daily CO_2 emission rate. The release of CO_2 over time (R) is expressed relative to the initial release of CO_2 (R_0). Each line represents the fit of a kinetic model to measured daily CO_2 emission rate data (pink circles).

and/or minerals. Although this hypothesis may have been met with some skepticism a decade ago, recent studies convincingly demonstrate the previously overlooked but crucial role of reactive minerals in the processing and transformation of soil OM (*37*). These durable catalysts can facilitate OM transformation by multiple processes, including electrolytic and/or hydrolytic decomposition of macromolecules, heterogeneous oxidation, and direct oxidation mediated by transition elements (e.g., Fe or Mn) (*29*, *37*). Redox-sensitive minerals, such as biotite, magnetite, Fe(II) sulfides, and Mn oxides, can induce the hydrolytic decomposition of large macromolecular organic molecules into small molecules and can also efficiently catalyze the transformation of OM into other molecules (*29*). For example, reactive Fe(II) has been shown to be the main driver of OM oxidation in floodplain soils, overtaking microbial activity (*38*). In addition, mineral nanozymes, which are nanosized mineral particles widely distributed in soils, are expected to play a critical role in the biogeochemical carbon cycle because of their strong catalytic activity (*39*, *40*). Magnetite nanoparticles, for example, have been shown to exhibit intrinsic enzyme-like activity similar to natural peroxidases, facilitating the oxidation of OM (*41*). Furthermore, electron transfer, which we have demonstrated in sterile soils (Fig. 4), can lead to the oxidation or reduction of OM compounds during mineral-mineral interactions in soil (*42*).

This study provides compelling evidence in support of the EXOMET hypothesis, showing that soil respiration can occur spontaneously, independent of cellular compartmentalization. In particular, we demonstrate the presence in sterile soils of (i) cascades of chemical reactions whose nature and dynamics depend on the supply and type of carbonaceous substrate; (ii) electron transfer originating from the carbonaceous substrate, with oxygen acting as the final electron acceptor; (iii) CO_2 emissions resulting from the decarboxylation of carbon isotope–labeled substrates; and (iv) the persistence of these oxidative metabolism-like catabolic reactions over a period exceeding 6 years.

Our study also enhances our understanding of EXOMET catalysts. By incubating a mixture of enzymes extracted from cells in water with glucose, we previously demonstrated that enzymes can generate respiratory activities without any cellular organization (*13*). However, these activities could only be maintained for a few hours to days, probably due to enzyme inactivation and/or incomplete metabolism and cofactor regeneration. This study shows that by maintaining the incubation of sterilized soils for years, nonenzymatic catalysts are also capable of generating respiratory activities, which persist for years as long as carbonaceous organic substrates are available. This persistence indicates the stable nature of these catalysts (e.g., metals) and the diverse reactions they can carry out (e.g., cleavage of various chemical bonds allowing deep oxidation of C compounds and electron transfers from organic C to O_2). Together, the results of our previous research (*12*, *13*) and this study suggest that EXOMETs in soils are catalyzed by a variety of enzymes and mineral catalysts with different lifetimes. These include free enzymes, enzymes bound to soil particles, and mineral catalysts.

Our findings have implications for understanding biogeochemical cycles in soils. They indicate that CO_2 emissions and O_2 consumption in soils depend on two distinct but interacting metabolisms, the respiration of living organisms and the EXOMETs. These two metabolisms must be explicitly considered when studying biogeochemical cycles, as they are unlikely to obey the same laws and respond differently to environmental factors. The metabolism of living organisms is designed to meet the nutritional and reproductive needs of organisms that have limited lifespans, have narrow physiological constraints (e.g., temperature and humidity), and are shaped by evolutionary processes. EXOMETs are not driven by ecological goals and are highly resistant to toxicity, high temperature, and pressure (*13*, *17*), probably due to the involvement of highly stable, nonenzymatic catalysts.

Downloaded from https://www.science.org on November 28, 2026

It is also notable that stochastic processes (e.g., random fluctuations in metabolite production and consumption rates, passive movements, or low exchange rates of metabolites) have a limited influence on the dynamics of metabolite assemblages in sterile soils, even in this last phase of experiments, showing that the soil matrix shapes transformations with properties similar to biochemical transformations, given that deterministic processes (e.g., preferential consumption of thermodynamically more available compounds) are a feature of the latter (*43*). This perspective offers interesting avenues for exploring fundamental questions of prebiotic chemistry, particularly with regard to the ability of minerals to catalyze sequences of metabolism-like reactions, which is the subject of debates. Some argue that given the complexity of the metabolic pathways, it is unlikely that metabolism-like chemical reaction sequences could be catalyzed by simple environmental catalysts (*44*, *45*). Others argue that the topology of glycolysis and the Krebs cycle is rooted in nonenzymatic chemistry and that the precursors of these metabolic pathways were catalyzed by abundant metal ions available on the primordial planet (*46*, *47*). For example, Fe^{2+} has been shown to be capable of catalyzing 29 reactions involved in glycolysis and the pentose phosphate pathway in living organisms under conditions similar to those presumed in the archaean ocean (*48*). Our study, which shows the nonenzymatic promotion of multiple reactions in successive sequences, supports a scenario of nonenzymatic metabolism–like networks on primitive Earth and their persistence in contemporary soil ecosystems.

MATERIALS AND METHODS

Soil sampling and soil sterilization

Soil samples were taken from the 5- to 20-cm soil layer at the Theix site (Massif Central, France). The soil is a sandy loam Cambisol developed on granitic rocks and has the following characteristics: pH_{water} 6.2; carbon content, 39 gC kg^{-1}; clay, 26%; silt, 25%; sand, 49%; cation exchange capacity, 21.5 cmol kg^{-1}. For detailed information on the sampling site and on soil characteristics, see the works of Fontaine *et al.* (*49*) and Kéraval *et al.* (*22*). The fresh soil samples were mixed, sieved at 2 mm, and dried to a moisture content of 5% (w/w of water per dry soil). The soil was packaged in small hermetically sealed plastic bags, which were then placed in two further lays of plastic bags. Soils were irradiated with gamma rays at a dose of 45 kGy (^{60}Co, IONISOS, ISO14001, France). This sterilization treatment effectively (i) suppresses active cells from soils (*12*, *13*, *20*), (ii) limits the impact of sterilization treatments on the physicochemical soil properties (*20*, *21*), and (iii) yields similar respiration rates over a 15-day incubation period to soil sterilized by both γ-irradiation and autoclaving (*12*).

Preparation of soil microcosms for the medium-term experiment (6 months)

The nonsterilized soil (hereafter referred to as LS) and IS microcosms consisted of 10 g of sieved soil samples (dry mass) placed in 120-ml sterile glass vials capped with butyl rubber stoppers and sealed with aluminum crimps. The microcosms are not affected by any physical disturbances once they are sealed and during the incubation period. Sterile solutions of uniformly labeled (i.e., all labeled positions) ^{13}C-glucose (CAS: 110187-42-3, Cambridge Isotope Laboratories) and ^{13}C-citrate (CAS: 287389-42-9, Aldrich) were prepared and either not amended (IS) or added (5% ^{13}C labeled) to the G-IS and C-IS microcosms, respectively, for a final concentration of glucose and citrate in a soil microcosm of 3 mgC g^{-1}. All microcosms were flushed with sterile free CO_2 gas (80% N_2 and 20% O_2) moistened with sterile water (LS and IS) or sterile ^{13}C-glucose and ^{13}C-citrate solutions (G-IS and C-IS) to a water content of 30%. The microcosms were then incubated in the dark at 20°C for 163 days. Four independent microcosm replicates per sampling date and treatment (IS, G-IS, and C-IS) were incubated for the sterilized soils. To prevent the direct impact of sterilization, particularly the production of free radicals, 1 year was allowed to elapse between γ-irradiation sterilization and soil rewetting. Rewetting the soil was considered to be T0 and brought the water potential of the soil microcosms back to −100 kPa (i.e., the optimal potential for aerobic microbial activity). Sampling of the vials for analysis began 0.2 days after rewetting (T1) and then at T2 (3 days), T3 (6 days), T4 (17 days), T5 (100 days), and T6 (163 days) of incubation. All manipulations were carried out under sterile conditions, and each sampling was destructive to avoid the contamination of the soil microcosms. For LS microcosms, the microcosms were flushed at 9, 23, and 50 days with filtered ambient air.

Preparation of soil microcosms for the long-term experiment (>6 years)

Experimental microcosms consisted of 20 g of γ-irradiated soil, which was incubated with 6 ml of water (S treatment) or 5 ml of water and 1 ml of ^{13}C-labeled glucose solution (S + G treatment). The glucose solution contained 60 mg of C-glucose per milliliter and was prepared by mixing unlabeled glucose with ^{13}C-labeled glucose (C_6 atom% $^{13}C = 99\%$) to give a final $\delta^{13}C$ of 3712‰. The glucose solution was sterilized by filtration at 0.2 µm. Three replicates were made for each treatment. The volume of the solutions was adjusted to incubate the soil at a water potential of −100 kPa. The soil microcosms were then incubated at 25°C for 2442 days. All manipulations were performed under sterile conditions. Once sealed, the microcosms were unaffected by any physical disturbances during the incubation period.

Soil sterility tests

Extraction of cells from soils

At the end of the incubation period ($t = 163$ days and $t = 2442$ days for the medium-term and long-term experiments, respectively), the cells were separated from soil particles for all soil microcosms. One gram of soil was mixed with 10 ml of pyrophosphate buffer (1× phosphate-buffered saline and 0.01 M $Na_4P_2O_7$) and shaken on ice at 70 rpm on a rotary shaker for 30 min. After shaking, the solution was sonicated three times (1 min each) in a water bath sonicator (Fisher Bioblock Scientific 88156, 320W, Illkirch, France). The largest particles were removed by centrifugation (800*g*, 1 min), and the supernatant was stored at 4°C for 2 hours before quantification analysis.

Live/dead cell staining coupled to flow cytometry analysis

Samples were diluted in filtered tris-EDTA buffer (<0.2 µm) and stained with 1× SYBR Green I (S7585, Invitrogen), a cell-permeable DNA dye that stains all live and dead cells. Cells were also stained with propidium iodide (10 µg/ml; P4864, MERCK KGaA), a cell-impermeable DNA dye that exclusively stains dead cells (*50*), for 15 min in the dark at room temperature. Flow cytometry measurements were performed using a FACSAria Fusion SORP (BD Biosciences) equipped with a 70-µm nozzle and a 1.5 neutral density filter in a two-laser configuration depending on the dyes used (488 nm, 50 mW; and 561 nm, 50 mW). The respective fluorescence emissions were collected with long-pass (LP) and band-pass (BP) filter sets: 502-nm

Downloaded from https://www.science.org on November 28, 2026

LP/530/30-nm BP (SYBR Green I); 600-nm LP/610/20-nm BP (propidium iodide). The threshold was set at the minimum fluorescence on the SYBR Green I parameter. Data were acquired and analyzed on logarithmic scales using FACSDiva 8 software (BD Biosciences).

Cultural approaches

For the long-term experiment (>6 years), soils extracted at the end of the experiment (t = 2442 days) from the different S and S + G microcosm replicates were plated on Luria-Bertani and malt extract agar plates to check whether colonies of prokaryotes or fungi formed on the surface of the agar plates. After incubating for 1 week at 25°C, no colonies were visible on the agar medium.

In parallel, at t = 2442 days, 1 g of bulk soil samples from each of the S and S + G microcosms and for nonsterilized soil (used as a positive control) was placed in flasks containing Luria-Bertani and malt extract broth. Cultures were incubated for 120 hours at 25°C with shaking. Cultures were analyzed by flow cytometry after live/dead staining.

Transmission electron microscopy (TEM)

For the long-term experiment (>6 years), bulk soil samples were analyzed by TEM at the end of the incubation period (t = 2442 days) to check for the presence of cells with preserved morphology in the soil aggregates, as previously described (*12*). Briefly, ultrathin soil sections (90 nm thick) were observed by TEM. Centrifugation (12,000*g* for 2 min) was performed after each step of the soil inclusion protocol to pellet the soil samples. Aliquots of soil (0.05 g) were fixed for 1 hour in 1.5 ml of cacodylate buffer solution (pH 7.4, containing 0.2 M cacodylate, 6% glutaraldehyde, and 0.15% ruthenium red). The soil was then washed three times with 0.1 M cacodylate buffer solution for 10 min. Postfixation was carried out using the 0.1 M cacodylate buffer containing 1% osmic acid. To facilitate the further penetration of propylene oxide, the soil was dehydrated using a gradient of ethanol solutions: 50% ethanol (3 × 5 min), 70% ethanol (3 × 15 min), and 100% ethanol (3 × 20 min). To improve resin permeation, the sample was incubated in a propylene oxide bath (3 × 20 min). To allow the sample to absorb the resin, it was incubated overnight in a bath containing a 1:1 ratio of propylene oxide and Epon 812 resin and then flipped over. After polymerization of the cast resin on the soil specimens (48 hours at 50°C), the narrow parts of the molded, impregnated aggregates were pyramided using a Reichert TM60 ultramill. Last, ultrathin sections (90 nm) were made using a diamond knife (Ultra 45°, MF1845, DiATOME Ltd., Biel/Bienne, Switzerland) on an Ultramicrotome Ultracut S (Reichert Jung Leica, Austria). The soil sections were collected on 400-mesh copper electron microscope grids, which were supported by a carbon-coated Formvar film (Pelanne Instruments, Toulouse, France). Each grid was negatively stained with 2% uranyl acetate for 30 s, rinsed twice with distilled water, filtered to 0.02 µm, and dried on filter paper. The soil ultrathin sections were analyzed using a JEM 1200-EX TEM (JEOL, Akishima, Japan).

Nontargeted metabolite profiling using ^{1}H NMR

Extraction of exometabolites from soil

Exometabolite extraction was performed using the method developed by Jenkins *et al.* (*51*), with some minor modifications. Briefly, 4 g of soil was extracted under sterile conditions in 24 ml of sterile Milli-Q water at 4°C for 1 hour with shaking on an orbital shaker (Stuart SB3). The tubes were then centrifuged at 4°C for 5 min at 3200*g*, after which the resulting supernatant was collected in fresh 50-ml conical tubes and centrifuged again. These supernatants were then filtered using Swinnex filtration units fitted with 25-mm-diameter GF/F filters (Whatman) previously grilled at 450°C for 4 hours and rinsed with 30 ml of sterile Milli-Q water. The resulting water-extractable metabolites were frozen at −20°C, lyophilized to dryness using a Christ ALPHA 1-2 LDplus, and then resuspended in 1.5 ml of ultrapure water (Milli-Q system). The samples were filtered using a centrifugal filter (Amicon Ultra-4, 3 kDa), which had been rinsed with 4 ml of sterile 0.1 M NaOH and 4 ml of sterile Milli-Q water. After centrifugation for 45 min (7500*g*; 4°C), the <3-kDa exometabolites were lyophilized again and stored at −80°C until analysis.

Analysis by ^{1}H NMR

1) Recipes for preparing ^{1}H NMR buffer: buffer 1 (300 mM phosphate buffer solution, pH 7.28): 100 ml of D_2O (CAS: 7789-20-0, Cortecnet), 1.601 g of KH_2PO_4 (CAS: 7778-77-0, Fluka Analytical), 3.176 g of K_2HPO_4 (CAS: 7758-11-4, Fluka Analytical), 80 mg of reference molecule (TSP-d_4; CAS: 24493-21-8, Sigma-Aldrich), and 40 mg of NaN_3 (CAS: 26628-22-8, Sigma-Aldrich); buffer 2 (EDTA-d_{12} solution at 10 mM): 28.9 mg of EDTA-d_{12} [304 g mol^{-1}, ethylenediaminetetraacetic-d_{12} acid (98 atom %), CD650P1, COR-TECNET] and 10 ml of buffer 1 ; buffer 3: 10 ml of buffer 2, 5.5 ml of buffer 1, and 31 ml of D_2O, final pH 7.25.

2) Sample preparation: Each tube of dry sample was filled with 600 µl of buffer 3, vortexed, and transferred to a 5-mm-diameter NMR tube (InnovaChem SAS, B-500-5-7).

3) ^{1}H NMR spectral acquisition: ^{1}H NMR spectra were recorded at 298 K on a Bruker AVANCE III 500-MHz spectrometer equipped with a Bruker 5-mm Prodigy inverse cryoprobe probe TXI (^{1}H/^{13}C/^{15}N) with a *z*-gradient coil probe (Bruker Biospin GmbH). A one-dimensional ^{1}H NMR spectrum was acquired for all samples using a ZGPR sequence (with low-power presaturation of the water frequency). A total of 128 scans were collected with a 90° impulsion time of 9.94 µs at a power of 8.5 W, a relaxation time of 5 s, an acquisition time of 3.3 s, a spectral window of 20 ppm, and data points from 65 K filled from zero to 131 K before Fourier transformation with a line broadening of 0.3 Hz. All processing was performed using Bruker TopSpin 4.0.7. The NMR facility is ISO9001 certified.

4) Analysis of ^{1}H NMR spectra: The NMR spectra were imported and analyzed using NMRProcFlow 1.4.20 software (https://nmrprocflow.org/). The spectra were aligned locally and manually by the study group. Bucketing was performed using a peak-by-peak method with variable bucket sizes. The data matrix was normalized to the reference molecule bucket and a signal-to-noise ratio threshold of 3. PCA was performed using MetaboAnalyst 5.0 software (www.metaboanalyst.ca/) (*52*). Four replicate blanks were analyzed for each sampling date. A blank is defined as a sterilized water sample that has undergone all exometabolite extraction steps, sample preparation, and ^{1}H NMR analysis. The order in which the samples were analyzed was completely randomized.

For comparisons between treatments (IS, C-IS, and G-IS), a baseline correction was applied. To reduce the effect of glucose or citrate on the overall variance, we excluded, from the NMR spectrum, the regions [3.20 to 3.30 ppm], [3.35 to 3.94 ppm], [4.63 to 4.68 ppm], and [5.21 to 5.25 ppm], which correspond to α-glucose and β-glucose, and the region [2.48 to 2.76 ppm], which corresponds to citrate based on commonly used values for these molecules (*53*). We acknowledge that these zones may contain other molecules of interest.

5) Molecular richness and α-diversity: Although the concept of diversity is primarily used to describe organisms, ecological diversity

Downloaded from https://www.science.org on November 28, 2026

indices have been shown to be useful descriptors of the diversity of organic molecules in soils (*28*). For the water-extractable fraction of exometabolites with molecular weights <3 kDa, we calculated molecular richness using the sum of non-null buckets in each sample and the α-diversity using the Shannon-Wiener index (*54*) based on the relative abundance of buckets, which was calculated from the sum of peaks intensities. α-diversity indices were calculated using the QIIME workflow (*55*) on Galaxy (https://usegalaxy.fr/).

6) Data and statistical analyses: Statistical analyses were performed using GraphPad Prism version 8.0.1 (GraphPad Software Inc). For PCA, clustering and heatmaps were performed using MetaboAnalyst 5.0 software (www.metaboanalyst.ca/).

Gas flux measurements and isotopic composition of CO_2

Concentrations of CO_2 and O_2

For the medium-term experiment, gas-phase samples were taken from the LS, IS, C-IS, and G-IS vials at 0.2, 3, 6, 17, 100, and 163 days of incubation to measure CO_2 and O_2 concentrations. For the long-term experiment, CO_2 accumulation was measured in the gas phase of S and S + G microcosms after 0.5, 3.5, 10, 19, 53, 142, 1125, 1606, and 2442 days of incubation. Analyses were carried out using a Chrompack 438 gas chromatograph (Packard Instruments, Downers Grove, IL). Results are expressed as a percentage (%) corresponding to 1/10,000 ppm.

Isotopic composition of CO_2

The oxidation of the ^{13}C-labeled substrate was specifically quantified by monitoring the production of ^{13}C-labeled CO_2. The amount of CO_2 produced and its isotope composition ($\delta^{13}C$) were quantified using a cavity ring-down spectrometry analyzer coupled to a small sample injection module (Picarro G2101-i analyzer coupled to the small sample introduction module, Picarro Inc., Santa Clara, CA). The analyzer sampled a volume of 20 ml of gas. The CO_2 concentration in the gas samples ranged from 300 to 2000 ppm of CO_2 in accordance with the operating range of the analyzer. The CO_2 concentration and $\delta^{13}C$-CO_2 value of the gas samples were measured at a frequency of 0.5 Hz for 10 min. The analyzer provides an integrated value over this 10 min of measurement. A reference gas with a known concentration of CO_2 and $\delta^{13}C$ value was injected between the samples. Gas samples were diluted with synthetic air (O_2, 20%; N_2, 80%) when the CO_2 concentration exceeded the operating range of the analyzer. For the long-term experiment specifically, the cumulative amount of CO_2 was divided by the duration of each incubation period (in days) to calculate the average CO_2 emission rate. This was expressed as C-CO_2 (µmol of C released in the form of CO_2) per day per incubation flask. After gas analysis in the long-term experiment, the flasks were flushed with moistened synthetic air (O_2, 20%; N_2, 80%), which was sterilized by filtration at 0.2 µm.

Contribution of specific amendment to CO_2 emissions

The contribution of each amendment (glucose or citrate) to CO_2 emissions was determined using the following isotopic dilution equations

$$CO_{2\ soil} + CO_{2\ amendment} = CO_{2\ total} \quad (1)$$

$$CO_{2\ soil} \times A_{soil} + CO_{2\ amendment} \times A_{amendment} = CO_{2\ total} \times A_{total} \quad (2)$$

which leads to the following equation

$$CO_{2\ amendment} = CO_{2\ total} \times \left[\left(A_{total} - A_{soil}\right) / \left(A_{amendment} - A_{soil}\right)\right] \quad (3)$$

with $CO_{2\ soil}$ being the amount of CO_2 released from soil carbon, $CO_{2\ amendment}$ being the amount of CO_2 released from amendment (glucose or citrate), A_{soil} being the abundance of soil C, $A_{amendment}$ being the abundance of amended soil C, and A_{total} being the abundance of amended soil C and of soil carbon.

A is the isotope abundance: $A = R/(1 + R)$, with $A_{amendment} = 0.05$. R is the isotope ratio: $R = (^{13}C/^{12}C)$. $R_{sample} = [(\delta^{13}C/1000) + 1] \times R_{reference}$, with $R_{reference}$ relative to Pee Dee Belemnite = 0.0112372 and $\delta^{13}C = [(R_{sample}/R_{reference}) - 1] \times 1000$.

Data and statistical analyses

Analyses were performed using GraphPad Prism software version 8.0.1. The ratio of CO_2 emissions between sterilized soil and non-sterilized soil at T2 and T6 was compared using Welch's analysis of variance (ANOVA) followed by Dunnett's multiple comparisons test.

Principle, design and fuel cell measurements

The principle of the fuel cell is based on a column of soil. The top part of the soil is exposed to oxygen in the air, while the bottom part is enclosed by a plastic tube (Fig. 4). This design creates an oxygen gradient that decreases from the top of the cell (the cathode) to the bottom of the cell (the anode), which is similar to the gradient found in soil. This gradient promotes the capture of the electrons produced by the oxidation of organic molecules at the anode and their subsequent transfer to the cathode. The protons released during the oxidation of organic molecules diffuse through the soil column to reach the cathode, where they combine with oxygen to form water. The current induced by the transfer of electrons from the degradation of organic C to oxygen is measured using an amperemeter and a voltmeter. Soil contains a variety of organic and inorganic molecules that can respond to this oxygen gradient and generate electron flow by ways other than the oxidation of organic molecule (e.g., oxidation of Fe^{2+} to Fe^{3+}). To demonstrate the link between the oxidation of organic molecules and the electron flow, the current induced by the cell was measured with and without the addition of pyruvate.

Soil matrix preparation

Samples were collected from the 0- to 20-cm soil layer at the Theix site. The fresh soil samples were mixed, sieved at 2 mm, dried to a moisture content of 5% (w/w of water per dry soil), and then irradiated with gamma rays at a dose of 45 kGy (^{60}Co, IONISOS, ISO14001, France). The soil was packaged in small hermetically sealed plastic bags, which were then placed in two further lays of plastic bags. The soil samples were stored at 20°C for 4.8 years before being used to construct the air breathing cells. This period is long enough for cell debris to become invisible under electron microscopes (*12*) and for enzymes to become inactive (*13*).

Preparation of the fuel cell

The fuel cell was constructed using a 3-cm-diameter, 11-cm-high polypropylene Falcon plastic tube with a 50-ml capacity (Fig. 4). Holes were pierced in the bottom of the tube and the cap, and a graphite rod with a diameter of 2 mm was glued in place. These rods collect and transfer electrons to the anode and cathode of the fuel cell, respectively. The rods were covered with 10 cm^2 of carbon cloth to improve contact with the soil reactor and electron collection/distribution. Before assembly, the tube with the bonded electrodes and the pieces of carbon cloth were autoclaved at 121°C for 20 min.

Assembly of the fuel cell

All the manipulations were performed under a laminar flow hood. Three treatments were set up, including (i) sterilized soil with a sterile solution of sodium pyruvate (50 mM, Sigma-Aldrich Reagent Plus

Downloaded from https://www.science.org on November 28, 2026

≥99.9%, CAS: 113-24-6), (ii) sterilized soil with sterile water, and (iii) sterilized soil with a sterile solution of NaCl (50 mM, R.P. Normapur analytical reagent ≥99.5%). Treatments (ii) and (iii) served as controls for treatment (i), which was designed to investigate the impact of a readily degradable carbon supply on electron flow. Two injections of sodium pyruvate were administered for treatment (i), the first on day 0 and the second on day 77 of incubation. The same volume of water was added for the controls. Three replicates of each treatment were made. A volume of 16 ml of one of the three solutions was poured into the fuel cell, and then to avoid air bubbles, 37.5 g of sterilized soil (fresh weight basis, 4% moisture) was slowly poured in. The carbon tissue was placed on the surface of the wet soil. The tube cover was then screwed on, with the cathode carbon electrode threaded through the hole in the cover and placed on the soil surface.

Electrochemical characterization of the fuel cell

All fuel cells were tested using a precision digital multimeter (UNI-T-DT830B) to measure voltage (V) and current (I). The open circuit potential, current, and electrical power of the fuel cells connected to a 476-ohm resistor were measured at 0.08, 0.7, 1.0, 1.75, 3.0, 6.0, 9.0, 13.5, 19.5, 28.0, 77.0, 78.0, and 80.0 days of incubation. The electromotive force and fuel cell resistance were also determined by connecting the fuel cell to decreasing resistances (from 330 to 11,900 ohms) on day 9 for the water and sodium pyruvate treatments.

Data and statistical analyses

Analyses were performed with GraphPad Prism software version 8.0.1. Comparisons were based on two-way repeated measures ANOVA with Sidak's post hoc test for multiple comparisons.

Modeling the long-term dynamics of the rate of CO_2 emission observed in IS supplied with glucose (S + G)

The long-term dynamics of the CO_2 emission rate were analyzed using statistical modeling. Six different models were successively fitted to the decrease in CO_2 activity over time to investigate whether the fast and slow phases of the decrease were due to the activity of non-cellular catalysts with different kinetics.

These models were fitted to the observed CO_2 emission rate in the glucose-supplied mesocosms, in which substrate-limiting conditions were minimized. The models were designed primarily to test the possible involvement of catalysts of different types and lifespans in the oxidation of OM in sterilized soils.

Model 1 describes a simple exponential decrease in CO_2 activity with a constant decay rate k. Models 2 to 5 combine two exponentially decreasing CO_2 activities with fast (k_1) and slow (k_2) decay rates. While the decay rate of the slow kinetics (k_2) was fitted to the data in model 2, in models 3 and 4, it was forced to values giving half-lives of 43 and 495 days, respectively, corresponding to the estimates of Maire *et al.* (*13*) for long-term stabilized enzyme pools. Similarly, the value of k_2 was constrained in model 5 to an extremely high, albeit hypothetical, half-life of 7 years, which has never been observed for an enzyme pool. Last, model 6 combines a rapid exponential decrease in CO_2 emission rate with constant slow activity maintained throughout the long-term dynamics.

The models were fitted using the nls function from the lme4 R package (https://CRAN.R-project.org/package=lme4). For models 2 to 5, the "port" algorithm was used as an nls parameter to constrain k_1 estimates to values greater than the second activity kinetics decay rate. Figure 6A shows the model equations and all the statistical results obtained after fitting the models to the data. Only models 1, 4, 5, and 6 produced significant estimates. These competing models were then compared using the Akaike information criterion (AIC) to identify the best models. Figure 6B shows the observed and simulated data for models 1, 3, 4, and 6.

Supplementary Materials

This PDF file includes:

Figs. S1 to S7
Table S1

REFERENCES AND NOTES

1. J. W. Raich, W. H. Schlesinger, The global carbon dioxide flux in soil respiration and its relationship to vegetation and climate. *Tellus B Chem. Phys. Meteorol.* **44**, 81–99 (1991).
2. A. Nissan, U. Alcolombri, N. Peleg, N. Galili, J. Jimenez-Martinez, P. Molnar, M. Holzner, Global warming accelerates soil heterotrophic respiration. *Nat. Commun.* **14**, 3452 (2023).
3. P. M. Cox, R. A. Betts, C. D. Jones, S. A. Spall, I. J. Totterdell, Acceleration of global warming due to carbon-cycle feedbacks in a coupled climate model. *Nature* **408**, 184–187 (2000).
4. B. Bond-Lamberty, A. Thomson, Temperature-associated increases in the global soil respiration record. *Nature* **464**, 579–582 (2010).
5. C. E. Hicks Pries, C. Castanha, R. C. Porras, M. S. Torn, The whole-soil carbon flux in response to warming. *Science* **355**, 1420–1423 (2017).
6. H. Lundegårdh, Carbon dioxide evolution of soil and crop growth. *Soil Sci.* **23**, 417–453 (1927).
7. S. J. Kemmitt, C. V. Lanyon, I. S. Waite, Q. Wen, T. M. Addiscott, N. R. A. Bird, A. G. O'Donnell, P. Brookes, Mineralization of native soil organic matter is not regulated by the size, activity or composition of the soil microbial biomass—A new perspective. *Soil Biol. Biochem.* **40**, 61–73 (2008).
8. Y. Kuzyakov, E. Blagodatskaya, S. Blagodatsky, Comments on the paper by Kemmitt et al. (2008) 'Mineralization of native soil organic matter is not regulated by the size, activity or composition of the soil microbial biomass—A new perspective' [Soil Biology & Biochemistry 40, 61–73]: The biology of the Regulatory Gate. *Soil Biol. Biochem.* **41**, 435–439 (2009).
9. A. J. Ramsay, A. D. Bawden, Effects of sterilization and storage on respiration, nitrogen status and direct counts of soil bacteria using acridine orange. *Soil Biol. Biochem.* **15**, 263–268 (1983).
10. R. Lensi, C. Lescure, C. Steinberg, J.-M. Savoie, G. Faurie, Dynamics of residual enzyme activities, denitrification potential, and physico-chemical properties in a γ-sterilized soil. *Soil Biol. Biochem.* **23**, 367–373 (1991).
11. J. T. Trevors, Sterilization and inhibition of microbial activity in soil. *J. Microbiol. Methods* **26**, 53–59 (1996).
12. B. Kéraval, A.-C. Lehours, J. Colombet, C. Amblard, G. Alvarez, S. Fontaine, Soil carbon dioxide emissions controlled by an extracellular oxidative metabolism identifiable by its isotope signature. *Biogeosciences* **13**, 6353–6362 (2016).
13. V. Maire, G. Alvarez, J. Colombet, A. Comby, R. Despinasse, E. Dubreucq, M. Joly, A.-C. Lehours, V. Perrier, T. Shahzad, S. Fontaine, An unknown oxidative metabolism substantially contributes to soil CO_2 emissions. *Biogeosciences* **10**, 1155–1167 (2013).
14. H. Santruckova, M. I. Bird, J. L. Lloyd, Microbial processes and carbon-isotope fractionation in tropical and temperate grassland soils. *Funct. Ecol.* **14**, 108–114 (2000).
15. G. Wang, Y. Jia, W. Li, Effects of environmental and biotic factors on carbon isotopic fractionation during decomposition of soil organic matter. *Sci. Rep.* **5**, 11043 (2015).
16. G.-H. Yu, Y. Kuzyakov, Fenton chemistry and reactive oxygen species in soil: Abiotic mechanisms of biotic processes, controls and consequences for carbon and nutrient cycling. *Earth Sci. Rev.* **214**, 103525 (2021).
17. J. C. Blankinship, C. A. Becerra, S. M. Schaeffer, J. P. Schimel, Separating cellular metabolism from exoenzyme activity in soil organic matter decomposition. *Soil Biol. Biochem.* **71**, 68–75 (2014).
18. R. G. Efremov, L. A. Sazanov, Respiratory complex I: 'Steam engine' of the cell? *Curr. Opin. Struct. Biol.* **21**, 532–540 (2011).
19. T. V. Denisova, K. S. Kazeev, Sensitivity of some groups of ordinary chernozem soil microorganisms to γ irradiation. *Russ. J. Ecol.* **39**, 99–104 (2008).
20. N. McNamara, H. Black, N. Bresford, N. Parekh, Effects of acute gamma irradiation on chemical, physical and biological properties of soils. *Appl. Soil Ecol.* **24**, 117–132 (2003).
21. K. Lees, M. Fitzsimons, J. Snape, A. Tappin, S. Comber, Soil sterilisation methods for use in OECD 106: How effective are they? *Chemosphere* **209**, 61–67 (2018).
22. B. Kéraval, S. Fontaine, A. Lallemant, S. Revaillot, H. Billard, G. Alvarez, F. Maestre, C. Amblard, A.-C. Lehours, Cellular and non-cellular mineralization of organic carbon in soils with contrasted physicochemical properties. *Soil Biol. Biochem.* **125**, 286–289 (2018).

Downloaded from https://www.science.org on November 28, 2026

23. T. L. Swenson, U. Karaoz, J. M. Swenson, B. P. Bowen, T. R. Northen, Linking soil biology and chemistry in biological soil crust using isolate exometabolomics. *Nat. Commun.* **9**, 19 (2018).
24. Y. Song, S. Yao, X. Li, T. Wang, X. Jiang, N. Bolan, C. R. Warren, T. R. Northen, S. X. Chang, Soil metabolomics: Deciphering underground metabolic webs in terrestrial ecosystems. *Eco. Environ. Health* **3**, 227–237 (2024).
25. A. Malik, G. Gleixner, Importance of microbial soil organic matter processing in dissolved organic carbon production. *FEMS Microbiol. Ecol.* **86**, 139–148 (2013).
26. O. Beckonert, H. C. Keun, T. M. D. Ebbels, J. G. Bundy, E. Holmes, J. C. Lindon, J. K. Nicholson, Metabolic profiling, metabolomic and metabonomic procedures for NMR spectroscopy of urine, plasma, serum and tissue extracts. *Nat. Protoc.* **2**, 2692–2703 (2007).
27. J. Marchand, E. Martineau, Y. Guitton, B. Le Bizec, G. Dervilly-Pinel, P. Giraudeau, A multidimensional ^{1}H NMR lipidomics workflow to address chemical food safety issues. *Metabolomics* **14**, 60 (2018).
28. R. Davenport, B. P. Bowen, L. M. Lynch, Decomposition decreases molecular diversity and ecosystem similarity of soil organic matter. *Proc. Natl. Acad. Sci. U.S.A.* **120**, e2303335120 (2023).
29. M. Kleber, I. C. Bourg, E. K. Coward, C. M. Hansel, S. C. B. Myneni, N. Nunan, Dynamic interactions at the mineral-organic matter interface. *Nat. Rev. Earth Environ.* **2**, 402–421 (2021).
30. M. Spohn, K. Diáková, F. Aburto, S. Doetterl, J. Borovec, Sorption and desorption of organic matter in soils as affected by phosphate. *Geoderma* **405**, 115377 (2022).
31. T. L. Swenson, B. P. Bowen, P. S. Nico, T. R. Northen, Competitive sorption of microbial metabolites on an iron oxide mineral. *Soil Biol. Biochem.* **90**, 34–41 (2015).
32. C. Bouquet, M. Traïkia, F. Perrière, B. Kéraval, G. Alvarez, L. Louis, M. Leremboure, G. Voyard, S. Fontaine, A.-C. Lehours, Long lasting non-cellular reactions in sterile soils recapitulate most of the intermediates of the Krebs cycle. bioRixv 667751 [Preprint] (2025).
33. J. Piera, J. E. Bäckvall, Catalytic oxidation of organic substrates by molecular oxygen and hydrogen peroxide by multistep electron transfer—A biomimetic approach. *Angew. Chem. Int. Ed. Engl.* **47**, 3506–3523 (2008).
34. R. A. Barbato, K. L. Foley, J. A. Toro-Zapata, R. M. Jones, C. M. Reynolds, The power of soil microbes: Sustained power production in terrestrial microbial fuel cells under various temperature regimes. *Appl. Soil Ecol.* **109**, 14–22 (2017).
35. N. Fanin, M. Mooshammer, M. Sauvadet, G. Alvarez, L. Bernard, I. Bertrand, E. Blagodatskaya, L. Bon, S. Fontaine, S. Niu, G. Lashermes, T. L. Maxwell, M. N. Weintraub, L. Wingate, D. Moorhead, A. T. Nottingham, Soil enzymes in response to climate warming: Mechanisms and feedbacks. *Funct. Ecol.* **36**, 1378–1395 (2022).
36. J. Yan, G. Pan, L. Li, G. Quan, C. Ding, A. Luo, Adsorption, immobilization, and activity of β-glucosidase on different soil colloids. *J. Colloid Interface Sci.* **348**, 565–570 (2010).
37. S. Wu, K. O. Konhauser, B. Chen, L. Huang, "Reactive Mineral Sink" drives soil organic matter dynamics and stabilization. *npj Mater. Sustain.* **1**, 3 (2023).
38. H. R. Naughton, B. B. Tolar, C. Dewey, M. Keiluweit, P. S. Nico, S. Fendorf, Reactive iron, not fungal community, drives organic carbon oxidation potential in floodplain soils. *Soil Biol. Biochem.* **178**, 108962 (2023).
39. H. Wei, E. Wang, Nanomaterials with enzyme-like characteristics (nanozymes): Next-generation artificial enzymes. *Chem. Soc. Rev.* **42**, 6060–6093 (2013).
40. Z.-L. Chi, G.-H. Yu, Nanozyme-mediated elemental biogeochemical cycling and environmental effects. *Sci. China Earth Sci.* **64**, 1015 (2021).
41. L. Gao, J. Zhuang, L. Nie, J. Zhang, Y. Zhang, N. Gu, T. Wang, J. Feng, D. Yang, S. Perett, X. Yan, Intrinsic peroxidase-like activity of ferromagnetic nanoparticles. *Nat. Nanotechnol.* **2**, 577–583 (2007).
42. A. Qian, Y. Lu, Y. Zhang, C. Yu, P. Zhang, W. Liao, Y. Yao, Y. Zheng, M. Tong, S. Yuan, Mechanistic insight into electron transfer from Fe(II)-bearing clay minerals to Fe (hydr) oxides. *Environ. Sci. Technol.* **57**, 8015–8025 (2023).
43. R. E. Danczak, R. K. Chu, S. J. Fansler, A. E. Goldman, E. B. Graham, M. M. Tfaily, J. Toyoda, J. C. Stegen, Using metacommunity ecology to understand environmental metabolomes. *Nat. Commun.* **11**, 6369 (2020).
44. F. A. Anet, The place of metabolism in the origin of life. *Curr. Opin. Chem. Biol.* **8**, 654–659 (2004).
45. A. Lazcano, S. L. Miller, On the origin of metabolic pathways. *J. Mol. Evol.* **49**, 424–431 (1999).
46. M. Keller, D. Kampjut, S. Harrison, M. Ralser, Sulfate radicals enable a non-enzymatic Krebs cycle precursor. *Nat. Ecol. Evol.* **1**, 83 (2017).
47. M. Ralser, An appeal to magic? The discovery of a non-enzymatic metabolism and its role in the origins of life. *Biochem. J.* **475**, 2577–2592 (2018).
48. M. A. Keller, A. V. Turchyn, M. Ralser, Non-enzymatic glycolysis and pentose phosphate pathway-like reactions in a plausible Archean ocean. *Mol. Syst. Biol.* **10**, 725 (2014).
49. S. Fontaine, S. Barot, P. Barré, N. Bdioui, B. Mary, C. Rumpel, Stability of organic carbon in deep soil layers controlled by fresh carbon supply. *Nature* **450**, 277–280 (2007).
50. L. C. Crowley, A. P. Scott, B. J. Marfell, J. A. Boughaba, G. Chojnowski, N. J. Waterhouse, Measuring cell death by propidium iodide uptake and flow cytometry. *Cold Spring Harb. Protoc.* **2016**, doi: 10.1101/pdb.prot087163 (2016).
51. S. Jenkins, T. L. Swenson, R. Lau, A. M. Rocha, A. Aaring, T. C. Hazen, R. Chakraborty, T. R. Northen, Construction of viable soil defined media using quantitative metabolomics analysis of soil metabolites. *Front. Microbiol.* **8**, 2618 (2017).
52. Z. Pang, G. Zhou, J. Ewald, L. Chang, O. Hacariz, N. Basu, J. Xia, Using MetaboAnalyst 5.0 for LC–HRMS spectra processing, multi-omics integration and covariate adjustment of global metabolomics data. *Nat. Protoc.* **17**, 1735–1761 (2022).
53. T. W.-M. Fan, Metabolite profiling by one- and two-dimensional NMR analysis of complex mixtures. *Prog. Nucl. Magn. Reson. Spectrosc.* **28**, 161–219 (1996).
54. A. E. Magurran, *Ecological Diversity and Its Measurements* (Princeton Univ. Press, 1988).
55. J. G. Caporaso, J. Kuczynski, J. Stombaugh, K. Bittinger, F. D. Bushman, E. K. Costello, N. Fierer, A. G. Peña, J. K. Goodrich, J. I. Gordon, G. A. Huttley, S. T. Huttley, S. T. Kelley, D. Knights, J. E. Koenig, R. E. Ley, C. A. Lozupone, D. McDonald, B. D. Muegge, M. Pirrung, J. Reeder, J. R. Sevinsky, P. J. Turnbaugh, W. A. Walters, J. Widmann, T. Yatsunenko, J. Zaneveld, R. Knight, QIIME allows analysis of high-throughput community sequencing data. *Nat. Methods* **7**, 335–336 (2010).

Acknowledgments

Funding: C.B. was supported by Ph.D. fellowship from the French Ministry of Education and Research. We thank the financial support of (i) the CNRS through the Mission pour les Initiatives transverses et interdisciplinaires (MITI) and through Projet Exploratoire Premier Soutien (PEPS) and the funding of the ISO-EXOMET and EXCEED projects and (ii) CAP 20-25 Isite of the University Clermont Auvergne and the funding of the EXOMET project. **Author contributions:** Conceptualization: B.K., A.-C.L., G.A., and S.F. Methodology: C.B., B.K., M.T., G.A., F.P., A.-H.L.J., H.B., J.C., S.R., S.F., and A.-C.L. Validation: C.B., B.K., M.T., G.A., F.P., A.-H.L.J., H.B., J.C., S.R., S.F., and A.-C.L. Formal analyses: C.B. and B.K. Investigation: C.B., B.K., M.T., G.A., F.P., A.-H.L.J., H.B., J.C., S.R., S.F., and A.-C.L. Visualization: C.B. and A.-C.L. Supervision: A.-C.L., S.F., and M.T. Writing—original draft: C.B. and A.-C.L. Writing—review and editing: C.B., A.-C.L., S.F., M.T., G.A., and B.K. Project administration: A.-C.L. and S.F. Funding acquisition: A.-C.L. **Competing interests:** The authors declare that they have no competing interests. **Data and materials availability:** All data needed to evaluate the conclusions in the paper are present in the paper and/or the Supplementary Materials.

Submitted 20 February 2025
Accepted 14 October 2025
Published 12 November 2025
10.1126/sciadv.adw9065

Downloaded from https://www.science.org on November 28, 2026

Science Advances

Nonliving respiration: Another breath in the soil?

Clémentin Bouquet, Benoit Kéraval, Mounir Traikia, Gaël Alvarez, Fanny Perrière, Anne-Hélène Le Jeune, Hermine Billard, Jonathan Colombet, Sandrine Revaillot, Sébastien Fontaine, and Anne-Catherine Lehours

Sci. Adv. **11** (46), eadw9065. DOI: 10.1126/sciadv.adw9065

View the article online
https://www.science.org/doi/10.1126/sciadv.adw9065
Permissions
https://www.science.org/help/reprints-and-permissions

Downloaded from https://www.science.org on November 28, 2026

Use of this article is subject to the Terms of service

Science Advances (ISSN 2375-2548) is published by the American Association for the Advancement of Science. 1200 New York Avenue NW, Washington, DC 20005. The title *Science Advances* is a registered trademark of AAAS.

Copyright © 2025 The Authors, some rights reserved; exclusive licensee American Association for the Advancement of Science. No claim to original U.S. Government Works. Distributed under a Creative Commons Attribution NonCommercial License 4.0 (CC BY-NC).